Surface Latent Heat Flux and Relationships with SST in CFS

Renguang Wu[1,*], Ben P. Kirtman[1, 2] and Kathy Pegion[1]

[1] *Center for Ocean-Land-Atmosphere Studies, Calverton MD*

[2] *RSMAS/MPO, University of Miami, Miami, FL*

NOAA CTB - COLA

Joint Seminar

Jan. 9, 2008

1. Introduction

The surface latent heat flux (LHF) is an important quantity in atmosphere-ocean interactions, of which studies show the surface evaporation-sea surface temperature (SST) feedback could contribute to the development of several climate modes (the Atlantic meridional mode, Chang et al. 1997; the Indian Ocean dipole/zonal mode, Saji et al. 1999 and Webster et al. 1999). The NCEP Climate Forecast System (CFS) is an ocean-land-atmosphere fully coupled dynamical system designed for short-term climate prediction (Saha et al. 2006). Since the CFS became operational in August 2004, it has been increasingly used for various climate studies. The CFS retrospective forecast data lend themselves to many studies beyond seasonal forecasts. Thus, it is important to evaluate the CFS performance in both simulation and forecast modes to learn how closely to the reality the atmosphere and ocean interact in the model. This can be done by diagnosing the LHF-SST relationship (Barsugli and Battisti 1998; Wu et al. 2006).

The present study compares mean and interannual variability of LHF and the LHF-SST correlation in a 50-year CFS simulation and in 24-year CFS retrospective forecasts (Saha et al. 2006) against proxies derived from observational datasets, including the Goddard Satellite-based Surface Turbulence Fluxes version 2 (GSSTF2) for the period 1988-2000 (Chou et al. 2003) and the NOAA optimum interpolation (OI) version 2 monthly mean SST starting from November 1981 (Reynolds et al. 2002). A 30-year SST forced simulation of the atmospheric model of the CFS, i.e., the Global Forecast System (GFS), is also analyzed to give the information of how different the coupled and forced simulations are regarding the LHF variability and the LHF-SST relationship. The SST forcing for the forced simulation is from the CFS simulation.

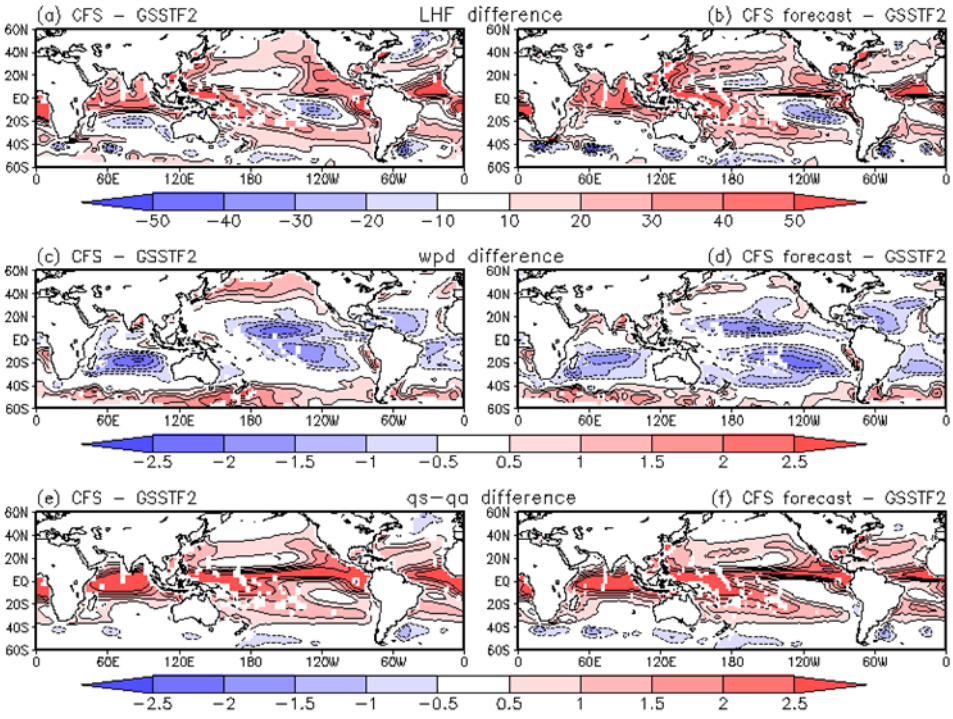

Figure 1 CFS simulation minus GSSTF2 differences of mean LHF (Wm^{-2}) (a), mean surface wind speed (m/s) (c), and mean sea-air humidity difference (g/kg) (e). (b), (d), and (f) are the same to (a), (c), and (e) except for the CFS retrospective forecasts with 1-month lead.

*Correspondence to: Renguang Wu, Center for Ocean-Land-Atmosphere Studies, 4041 Powder Mill Road, Suite 302, Calverton, MD 20705; E-mail: renguang@cola.iges.org

2. Mean and interannual variability

The distribution of mean LHF in GSSTF2 has been documented in previous studies (Chou et al. 2003; Feng and Li 2006). Large mean LHF is seen in trade wind belts and in the western boundary warm current regions of Kuroshio and Gulf Stream due to high surface winds coupled with large sea-air humidity differences. The LHF is also large in the Arabian Sea and the Bay of Bengal region in relation to the monsoon activity. Small LHF is seen in the eastern equatorial Pacific and Atlantic due to weak winds and upwelling-induced cold SSTs, and in high latitudes due to poleward decrease of SSTs. The LHF is also small in the equatorial eastern Indian Ocean-western Pacific warm pool region, mainly due to weak surface winds.

The CFS simulation and forecasts produces much larger LHF in the equatorial Indian Ocean-western Pacific, eastern equatorial Pacific, eastern tropical North Pacific, equatorial Atlantic, north of equatorial Atlantic, and in the western boundary current regions of Kuroshio and Gulf Stream (Figs. 1a-b). The difference of mean LHF in these regions exceeds 30 Wm-2. In trade wind belts, the CFS produces smaller LHF, especially in the South Pacific where the difference reaches about 20-30 Wm-2.

Higher LHF in the warm pool, cold tongue, and warm current regions is due to larger sea-air humidity difference (Figs. 1e-f). This, in turn, is attributed to lower surface air humidity (not shown). Higher LHF in the Bay of Bengal and northern Arabian Sea is due to higher wind speed (Figs. 1c-d). The wind speed in trade wind belts is weaker in the CFS, leading to smaller LHF in the subtropical South Indian and Pacific Oceans. In the mid-ocean part of the Pacific Inter-tropical Convergence Zone and western tropical North Atlantic, the effects of weaker trade winds are nearly cancelled by the effects of larger sea-air humidity difference.

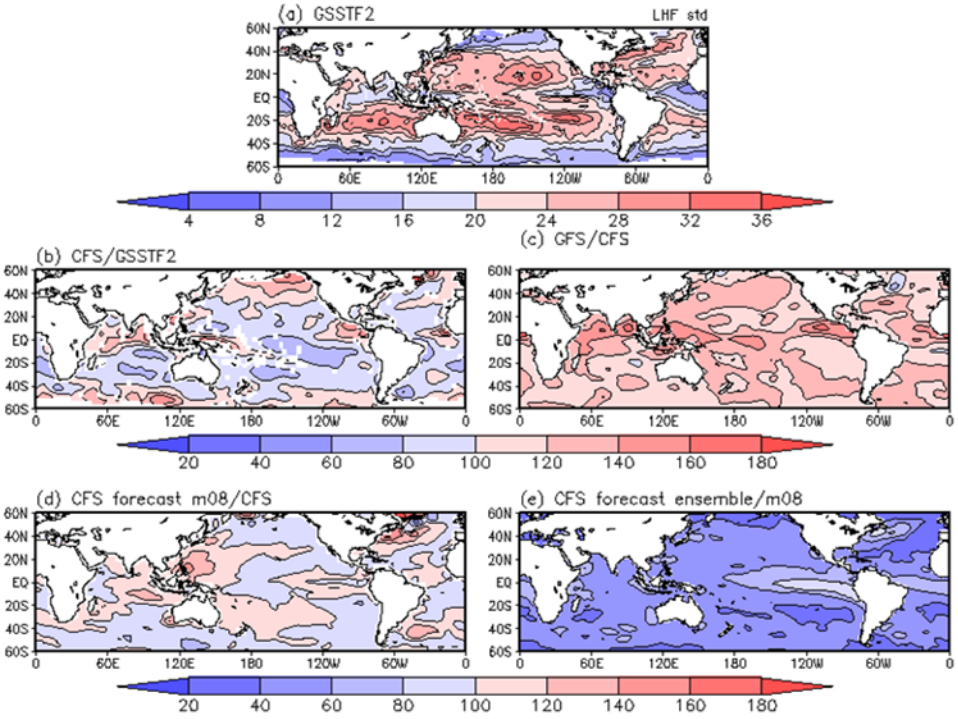

Figure 2 Standard deviation of monthly mean LHF anomalies (Wm^{-2}) from GSSTF2 (a), standard deviation ratio (%) of CFS simulation to GSSTF2 (b), GFS to CFS simulation (c), CFS individual forecast of 1-month lead to CFS simulation (d), and CFS ensemble forecast to individual forecast with 1-month lead (e).

Large LHF variability tends to occur in regions of high mean LHF because high mean wind speed and large sea-air humidity difference not only lead to high mean LHF, but also favor large LHF variability. In GSSTF2 (Fig. 2a), the variability is large over subtropical regions and western boundary warm current regions. The variability is small in eastern tropical Atlantic, eastern equatorial Pacific, and in high latitudes. The variability is relatively low in the equatorial eastern Indian Ocean and western Pacific.

Compared to GSSTF2, the CFS simulation (Fig. 2b) displays larger LHF variability in the equatorial Indian Ocean-western Pacific, coastal southeast China, tropical eastern North Pacific, tropical eastern North Atlantic. This is related to larger mean sea-air humidity difference in the CFS (Fig. 1e). The larger variability in high latitudes may be due to higher mean wind speed (Fig. 1c) and larger wind speed variability in the CFS. The

variability in trade wind belts is smaller in the CFS compared to GSSTF2, which is related to weaker mean wind speed (Fig. 1c) and smaller variability of sea-air humidity difference in the CFS.

Compared to the CFS coupled simulation, the SST forced GFS simulation (Fig. 2c) displays larger variability globally. The most pronounced variability increase is seen in the tropical Indian Ocean-western Pacific, eastern tropical North Pacific and Atlantic. The increase of variability in these regions reaches 40%. This increase is due to the lack of atmospheric negative feedback in the forced simulation, which increases the persistence of atmospheric anomalies and leads to excessively large seasonal mean rainfall and surface LHF anomalies (Wu and Kirtman 2005). This is most pronounced in regions of warm SST and high mean rainfall where the atmospheric internal dynamics is active and contributes to SST variations.

The individual CFS retrospective forecast displays a spatial distribution of LHF variability similar to the CFS coupled simulation. The difference in the magnitude of the LHF variability is within 20% in most regions (Fig. 2d). An increase over 20% is seen in the eastern tropical Indian Ocean, the western North Pacific and Atlantic.

The CFS forecast ensemble shows significantly reduced LHF variability, presumably due to ensemble averaging. The ensemble mean LHF variability is less than 60% of individual member in most of the regions (Fig. 2e). This suggests that the LHF has a large component of high frequency variations driven by atmospheric internal dynamics. The effects are smallest in the eastern equatorial Pacific, equatorial Atlantic, and mid-latitude western North Atlantic where the ocean forcing of the atmosphere dominates.

3. Latent heat flux-SST correlation

In observations (Fig. 3a), positive LHF-SST correlation is seen in the eastern equatorial Pacific and Atlantic, western North Pacific, western North Atlantic, tropical North Atlantic, southwest coast of Australia, and south of Africa. In the equatorial central-western Pacific and most of the tropical Indian Ocean, the correlation is negative. The LHF-SST tendency correlation is negative in mid-latitudes, equatorial central-western Pacific, north Indian Ocean, and coastal Sumatra (Figure 6c of Wu et al. 2006). The above distribution of correlation indicates the dominance of oceanic forcing of the atmosphere in the eastern equatorial Pacific and Atlantic, and the dominance of atmospheric forcing of the ocean in mid-latitudes and the contribution of atmospheric forcing to SST variations in the eastern Indian Ocean-western Pacific.

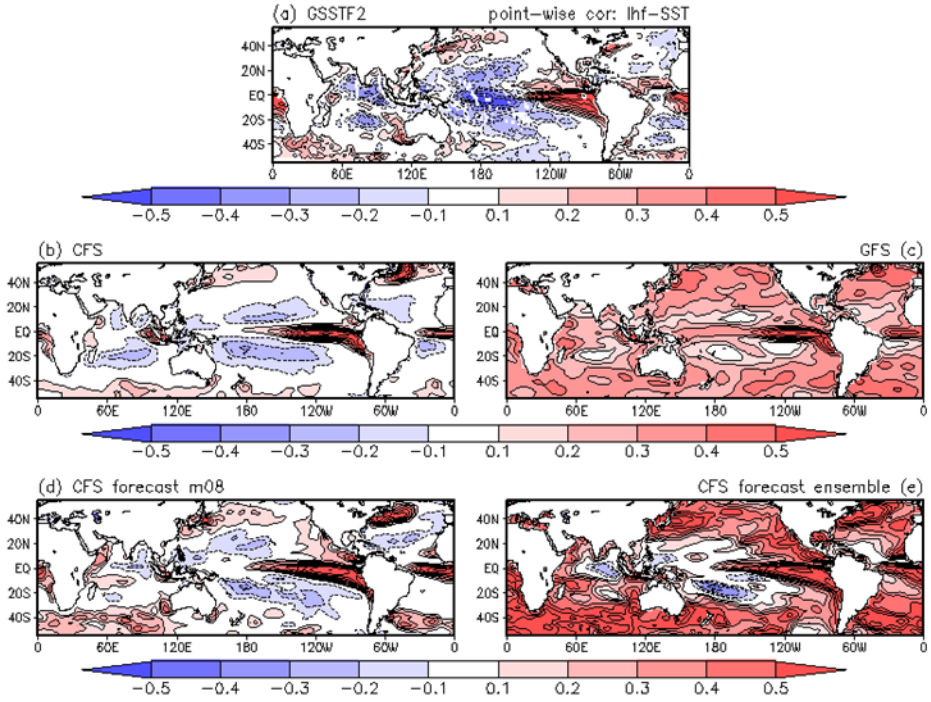

Figure 3 Point-wise and simultaneous LHF-SST correlation derived from GSSTF2 and OI version 2 SST (a), the CFS coupled simulation (b), the GFS forced simulation (c), an individual member of CFS forecasts of 1-month lead (d), and CFS ensemble forecasts of 1-month lead (e).

The CFS coupled simulation (Fig. 3b) captures the positive correlation in the eastern equatorial Pacific and Atlantic, and in the western North Pacific and North Atlantic, but misses the negative correlation in the

equatorial western-central Pacific. In particular, the simulation produces a positive correlation in the coastal Sumatra-Java region, which is in sharp contrast with observations. This positive correlation suggests the dominance of oceanic forcing of the atmosphere, as in the eastern equatorial Pacific and Atlantic. This disagrees with observations.

The GFS forced simulation (Fig. 3c) displays the dominance of positive LHF-SST correlation. This contrasts with the coupled simulation and indicates that the forced simulation produces spurious oceanic forcing of the atmosphere, consistent with previous studies (Wu et al. 2006).

The CFS individual forecast (Fig. 3d) displays LHF-SST correlation similar to the CFS simulation. There are, however, some regional differences. In the eastern tropical Indian Ocean, the positive LHF-SST correlation is limited in spatial coverage compared to the coupled simulation. When the forecast lead time increases, the positive correlation in the eastern Indian Ocean becomes more similar to the coupled simulation (not shown).

In the CFS ensemble forecasts (Fig. 3e), the LHF-SST correlation displays large differences from the individual forecast; the ensemble forecast has a much larger and broader positive correlation. This difference occurs because the ensemble averaging removes the high-frequency LHF variations that are weakly correlated with SST variations. The remaining low frequency LHF variations are largely induced by SST variations and thus have a positive correlation with SST. With the increase of forecast lead time, the spatial coverage of positive LHF-SST correlation is reduced in particular in mid-latitudes (not shown).

The discrepancy in the LHF-SST correlation is mainly due to excessive dependence of sea-air humidity difference on SST in the CFS simulation and forecast. This is confirmed by comparing the correlation between the sea-air humidity difference and SST. In the CFS coupled simulation and retrospective forecasts, the correlation between sea-air humidity difference and SST is very high (correlation coefficient > 0.7) (not shown). The corresponding correlation based on observations is below 0.5 except for eastern tropical Pacific and Atlantic.

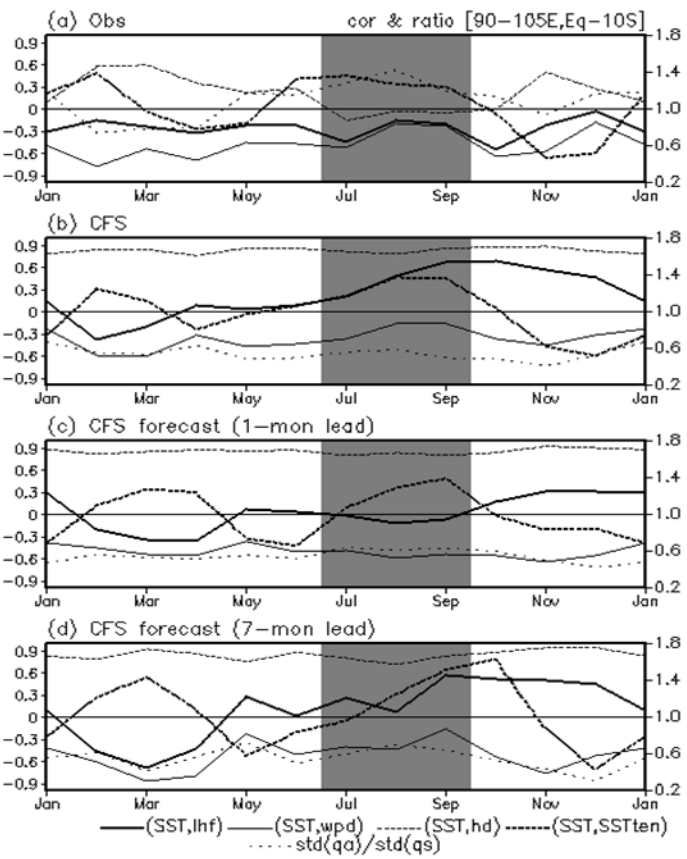

Figure 4 Point-wise and simultaneous correlation (scale at left) of LHF (thick solid), surface wind speed (thin solid), sea-air humidity difference (thin dashed), and SST tendency (thick dashed) with respect to SST, and ratio (dotted; scale at right) of standard deviation of surface air humidity to that of sea humidity, area averaged over the region of 5°S-5°N and 170°-90°W and derived from GSSTF2 and OI version 2 SST (a), the CFS coupled simulation (b), and CFS ensemble forecasts of 1-month lead (c) and 7-month lead (d).

4. Latent heat flux-SST relationship in the eastern equatorial Indian Ocean

Observational evidence indicates that the development of the Indian Ocean dipole/zonal mode during boreal summer involves a positive wind-evaporation feedback (Wang et al. 2003; Wu and Kirtman 2007). Can the CFS simulation or retrospective forecasts capture the positive wind-evaporation feedback in the above region? To address this question, we have calculated monthly simultaneous correlation with respect to SST anomalies for the region of 0°-10°S, 90°-105°E (Fig. 4).

The CFS simulation and CFS retrospective forecasts capture the SST warming during boreal summer although the positive SST tendency appears about 1-2 months later in the CFS forecasts. In observations, the LHF is reduced due to a decrease in wind speeds, indicating a positive feedback of evaporation on SST. In the CFS simulation, however, LHF anomalies are positive, i.e., surface evaporation has a damping effect on the existing warm SST anomalies, which is opposite to observations. This occurs because of the large positive correlation between sea-air humidity difference and SST. In the 1-mon lead CFS forecasts, LHF anomalies are weak because of the cancellation of sea-air humidity difference effects on the wind speed effects. When the forecast lead time increases to 7 months, LHF anomalies become positive as in the CFS simulation.

A common feature of the CFS simulation and retrospective forecasts is that the sea-air humidity difference follows closely the SST variation, whereas in observations the sea-air humidity difference is not as closely related to SST. This discrepancy occurs because the CFS has a dry bias in the eastern equatorial Indian Ocean that leads to smaller variability in the surface air humidity compared to that of sea humidity (Figs. 4b-d). As such, the sea-air humidity difference anomalies follow the sea humidity (or SST) anomalies. In observations, the variability of the air humidity is larger than that of the sea humidity (Fig. 4a).

5. Summary

The CFS mean LHF is higher than satellite estimates in the tropical Indo-western Pacific, tropical Atlantic, eastern tropical Pacific, and Kuroshio and Gulf Stream regions. This discrepancy is due to larger sea-air humidity difference. In the South Indian and Pacific Ocean trade wind belts, the CFS mean LHF is lower than satellite estimate due to weaker winds. The forced simulation produces a larger variability of LHF due to the lack of atmospheric negative feedback. The CFS ensemble forecasts have much smaller variability of LHF due to reduced high frequency variability.

The CFS simulations and retrospective forecasts display large discrepancy from observations in the local LHF-SST correlation in the eastern equatorial Indian Ocean and western-central equatorial Pacific. This discrepancy is due to an excessively large contribution of sea-air humidity difference to the LHF-SST correlation. The ensemble averaging in retrospective forecasts significantly increases the LHF-SST correlation in mid-latitudes.

The CFS simulation fails to capture the LHF-SST relationship in the eastern equatorial Indian Ocean. In observations, the wind-evaporation feedback contributes to the development of SST anomalies in the eastern pole of the Indian Ocean Dipole/Zonal Mode during boreal summer. In the CFS simulation, surface LHF acts as a damping term due to an excessive SST dependence in the sea-air humidity difference anomalies. While the short-lead CFS retrospective forecasts appear better than the CFS simulation in this aspect, this problem shows up when the forecast lead time increases.

The discrepancies between the CFS and observations in the eastern Indian Ocean-western Pacific are related to a dry bias in the CFS. The dry bias leads to lower variability in the surface air humidity because the interaction between convection and circulation depends on the mean state. As a result, the CFS underestimates the atmospheric forcing of SST, and overestimates the SST forcing of the atmosphere in the above regions. This suggests the importance of improving the simulation of mean moisture fields. The specific reasons for the dry bias remain to be uncovered.

References

Barsugli, J. J., and D. S. Battisti, 1998: The basic effects of atmosphere-ocean thermal coupling on midlatitude variability, *J. Atmos. Sci.*, **55**, 477-493.

Chang, C.-P., L. Ji, and H. Li, 1997: A decadal climate variation in the tropical Atlantic Ocean from thermodunamic air-sea interactions. *Nature*, **385**, 516-518,

Chou, S.-H., E. Nelkin, J. Ardizzone, R. M. Atlas, and C.-L. Shie, 2003: Surface turbulent heat and momentum fluxes over global oceans based on the Goddard Satellite retrievals, version 2 (GSSTF-2), *J. Climate*, **16**, 3256-3273.

Feng, L., and J. Li, 2006: A comparison of latent heat fluxes over global oceans for ERA and NCEP with GSSTF2, *Geophys. Res. Lett.*, **33**, L03810, doi:10.1029/2005GL024677.

Reynolds, R. W., N. A. Rayner, T. M. Smith, D. C. Stokes, and W. Wang, 2002: An improved in situ and satellite SST analysis for climate, *J. Climate*, **15**, 1609-1625.

Saha, S. and Coauthors, 2006: The NCEP Climate Forecast System, *J. Climate*, **19**, 3483-3517.

Saji, N. H., B. N. Goswami, P. N. Vinayachandran, and T. Yamagata, 1999: A dipole mode in the tropical Indian Ocean, *Nature*, **401**, 360-363.

Wang, B., R. Wu., and T. Li, 2003: Atmosphere-warm ocean interaction and its impacts on the Asian-Australian monsoon variation, *J. Climate*, **16**, 1195-1211.

Webster, P. J., A. M. Moor, J. P. Loschnigg, and R. R. Leben, 1999: Coupled ocean-atmosphere dynamics in the Indian Ocean during 1997-98, *Nature*, **401**, 356-360.

Wu, R., and B. P. Kirtman, 2005: Roles of Indian and Pacific Ocean air-sea coupling in tropical atmospheric variability, *Clim. Dyn.*, **25**, 155-170.

Wu, R., B. P. Kirtman, and K. Pegion, 2006: Local air-sea relationship in observations and model simulations, *J. Climate*, **19**, 4914-4932.

Wu, R., and B. P. Kirtman, 2007: Regimes of seasonal air-sea interaction and implications for performance of forced simulations, *Clim. Dyn.*, **29**, 393-410.